THE JOURNAL OF PHYSICAL CHEMISTRY C
A JOURNAL OF THE AMERICAN CHEMICAL SOCIETY

pubs.acs.org/JPCC

Article

Effect of Aqueous Electrolytes on $LiCoO_2$ Surfaces: Role of Proton Adsorption on Oxygen Vacancy Formation

Sergio Posada-Pérez, Geoffroy Hautier, and Gian-Marco Rignanese*

Cite This: *J. Phys. Chem. C* 2022, 126, 110−119

Read Online

ACCESS | Metrics & More | Article Recommendations | Supporting Information

ABSTRACT: Aqueous electrolytes are a safer, greener, and cheaper solution for energy storage applications. However, aqueous Li-ion batteries (ALIBs) suffer from faster degradation and poorer cyclability. The presence of H^+ and O loss have often been claimed to deteriorate electrode materials in aqueous electrolytes. Understanding the surface reactivity of the commercial $LiCoO_2$ cathode with respect to aqueous electrolytes and O loss is essential for designing cathode materials in such aqueous electrochemical cells. In this work, we use density functional theory calculations to investigate the stability and structure of several low-index surfaces of layered $Li_{1-x}CoO_2$ $(0 \leq x \leq 0.5)$ before and after H^+ adsorption. We compute the binding energies of H^+ from low to full coverage regimes. By employing ab initio atomistic thermodynamics, we determine the stability of O vacancies on protonated and nonprotonated layered $LiCoO_2$ surfaces. Our computations demonstrate that O loss is energetically favorable on the lowest energy surfaces, i.e., on the most exposed surface terminations. We suggest that the O vacancy formation is directly related to the transition metal (Co) coordination. Finally, the role of H^+ on O loss is investigated, showing that H^+ can facilitate the generation of O vacancies in some surface terminations.

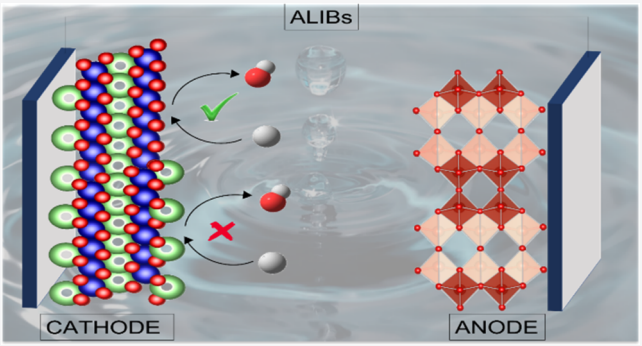

1. INTRODUCTION

Due to their excellent characteristics, lithium-ion batteries (LIBs) power most of our portable devices such as smartphones and laptops.[1,2] Despite this great success, unexpected fires and possible explosions have raised safety concerns. One culprit is the liquid electrolyte, a usually flammable organic solvent that ensures ionic mobility between the electrodes (cathodes and anodes).[3−5] To overcome these problems, electrolytes based on cheap inorganic salts in water have attracted considerable attention as a potential alternative due to their safety, low cost, environmentally friendly behavior, and large ionic conductivity in comparison to nonaqueous electrolytes.[6−9]

The overall electrochemistry of aqueous batteries is identical to that of conventional rechargeable ion batteries relying on organic electrolytes. Nonetheless, many issues have to be expected when switching from an organic electrolyte to water. First, the voltage window accessible to cathodes and anodes is limited by water decomposition through O_2 evolution at the cathode and H_2 evolution at the anode. This window is around 1.23 V[10,11] compared to organic electrolytes that can operate at higher voltages (3−4 V).[8] However, it can be pushed upward by introducing highly concentrated salts in water, producing so-called "water-in-salt" electrolytes. It can actually be brought close to that of organic electrolytes, thereby opening the way to a potential replacement of the organic electrolyte by an aqueous one.[12−15] Most of the water-in-salt electrolyte studies have focused on Li salts. Further improvements are needed to limit electrode degradation by selecting materials appropriate for aqueous batteries. It is well-known that the free water fraction is one of the key factors affecting the electrochemical stability of electrolytes.[16] The interaction of the electrodes with water leads to many deterioration mechanisms that are currently often hypothesized but not very well explored. One of them is the interaction with protons (H^+), which has been one of the common assumptions to explain performance issues in aqueous electrolytes due to their possible intercalation and degradation mechanisms.[17−19]

One of the most relevant cathode compounds for conventional LIBs is layered lithium cobalt oxide (LCO), whose commercialization was boosted by the pioneering work of Goodenough et al. in 1980.[20] Owing to its higher working potential, LCO is a very promising candidate as a cathode for aqueous LIBs.[21] Consequently, LCO and materials of the same family have been extensively investigated using aqueous electrolytes. Hydrothermal experiments in acidic media

Received: October 29, 2021
Revised: December 15, 2021
Published: December 27, 2021

https://doi.org/10.1021/acs.jpcc.1c09348
J. Phys. Chem. C 2022, 126, 110−119

corroborated by computational studies revealed that LCO is very prone to accommodate H^+ on Li^+ sites, which degrades the cathode due to the difficulty to (re)insert Li ions.[22−29] Nevertheless, cyclability experiments in aqueous electrolytes have shown a similar behavior as for organic electrolytes with excellent stability of LCO.[30,31] Though LCO bulk degradation was not observed during battery operations, a deterioration of the surface was detected due to O loss and cobalt oxide (CoO) formation.[31]

Oxygen vacancy formation (O_{vac}) is not unexpected during battery operations. In fact, O_{vac} can improve battery performance by promoting Li-ion diffusion and enhancing the capacity.[32,33] However, the O_{vac} formation can accelerate cathode degradation and phase transformations due to changes in the electronic structure and promotion of defects.[34−36] Understanding the mechanisms and processes for O_{vac} generation and the role of the aqueous electrolyte (mainly the H^+−cathode interaction) is crucial for designing cathode materials in aqueous batteries. In this framework, surface processes become a major concern. The O loss and the interaction with H^+ can affect the surface stability and promote surface reconstruction. Controlling O_{vac} formation and H^+ interaction with cathode surfaces is fundamental to improve the cathode performance.

In this work, we have carried out an extensive study of H^+ adsorption on the lowest energy LCO surface terminations relying on density functional theory (DFT). The latter is an effective and accurate method to study surface structures and vacancy defects.[37,38] We discuss the stability of O loss at LCO surfaces and the role of H^+ in the O_{vac} formation. Water adsorption at LCO surfaces has already been investigated in previous works, concluding that the presence of surface defects such as O_{vac} and Li antisites increases the LCO−water interaction.[39,40] Nevertheless, there is no information about the H^+−LCO interaction at the most exposed surface terminations and about the role of H^+ on the O_{vac} formation. This study provides a fundamental understanding of the interaction of LCO and water electrolytes at the surface level. This will help to precisely tailor the surface properties to enhance the optimized stability and performance of LCO in aqueous Li-ion batteries (ALIBs).

2. COMPUTATIONAL DETAILS

2.1. First-Principles Calculations. The periodic spin-polarized DFT calculations were performed using the Perdew−Burke−Ernzerhof (PBE) exchange−correlation functional.[41] The DFT+U formalism was used following the method suggested by Dudarev[42] to better describe the local character of the strongly correlated 3d electrons of the Co atoms. Following the scheme adopted in the Materials Project Database[43] for $LiCoO_2$, we chose a U value of 3.2 eV. All computations with Co are performed using a high-spin ferromagnetic initialization and allowing the spin relaxation.[43] The electronic density of the valence electrons was expanded onto a plane-wave basis set. The effects caused by the core electrons on the valence ones were described through the project augmented wave (PAW) method of Blöch[44] as implemented by Kresse and Joubert.[45] For electronic relaxation, the self-consistent loop was stopped when the total energy change was smaller than 10^{-5} eV. For atomic relaxation, minimization was interrupted as soon as the forces acting on the atoms were smaller than 0.01 eV $Å^{-1}$. To carry out the numerical integration in the Brillouin zone, a 5 × 5 × 1 Monkhorst−Pack mesh of k-points was employed.[46] All of the calculations were performed with the VASP code.[47]

2.2. Surface Models. Focusing on the low-index surfaces, bulk LCO can be cleaved to expose the polar (001) and (012) terminations and the nonpolar (104) and (110) surfaces. Their morphology has already been discussed in previous DFT studies.[48−50] The polar (001) and nonpolar (104) surfaces are most stable, as also found in experiments. Note, however, that the surface energy is sensitive to the Li chemical potential μ_{Li}, which is modified during LCO cyclability to promote the Li insertion/extraction process.[48] The nonpolar (110) presents the highest surface energy, i.e., it is the less stable cleavage surface.[50] In fact, it has been shown that surface stability is related to the coordination loss of the transition metal, which increases the surface energy.[51] As a result, LCO particles are terminated mainly by (001) planes, whereas (104) and (012) facets are predominant at the edges.[48,50]

In this work, we also deal with these four low-index surfaces. Our models are depicted in Figure S1. All our LCO slab models were constructed using eight $LiCoO_2$ formula units so that the corresponding supercells contain 8 Co and 16 O atoms. All of the models were generated starting from the relaxed bulk positions. The periodically repeated slabs are separated by more than 12 Å in all cases. The half-bottom atomic layers were relaxed while their bulk positions remain fixed.

For the two polar surfaces, reconstruction is required to redistribute the charge and generate stoichiometric slabs.[52] On the one hand, the (001) slab consists of monatomic layers with a repeated Li−O−Co−O pattern. Thus, Li, Co, and O terminations are possible. Co termination is the highest in energy due to the high cost for breaking the Co−O bond, as shown by previous DFT computations.[48,51,53] Li termination has been predicted lower in energy and is dependent on μ_{Li} since increasing and lowering μ_{Li} implies changes in surface energetics.[48] Merely cleaving the crystal at a Li plane would generate an infinite electric field. Indeed, the surface Li layer will display a positive (+1) charge, whereas the following O−Co−O layers will show a formal negative charge (−1). Instead, if the slab is terminated with half a monolayer of Li on each side, both surface layers are equally charged and the slab is nonpolar. In this way, Co remains octahedrally (6-fold) coordinated as in LCO bulk.[48,54] On the other hand, the polar (012) slab alternates cationic (Li−Co) and anionic (O) layers. The most stable reconstructed slab is terminated with half a monolayer of O atoms on both sides. It is again the one that minimizes the loss of coordination for the Co atoms (4-fold). Strictly speaking, the anions (O) and the cations (Li−Co) are not placed in the same layer. Nevertheless, in contrast to (001), the distance between anionic and cationic layers is very small as can be observed in Figure S1.

For both nonpolar surfaces, the three species are present in a stoichiometric ratio in each layer. Before optimization, the O atoms are outside the Li−Co plane for the (104) termination, but this difference is not significant. In fact, after atomic relaxation, the Co atoms are aligned with the O ones, whereas the Li cations are in a slightly lower position. It is also worth mentioning that the most exposed Co ions are 5- and 4-fold coordinated in the (104) and (110) slabs, respectively, in agreement with previous studies.

Finally, the partially delithiated surfaces were constructed by removing the most external Li atoms without modifying the surface termination but allowing the atomic displacement. The

https://doi.org/10.1021/acs.jpcc.1c09348
J. Phys. Chem. C 2022, 126, 110−119

fully lithiated $LiCoO_2$ surfaces contain 8 Li atoms, whereas the partially lithiated $Li_{0.75}CoO_2$ and $Li_{0.5}CoO_2$ surfaces contain 6 and 4 Li atoms, respectively. The partial delithiation does not induce any significant surface reconstruction.

2.3. Surface Energies of Clean Slabs. The surface free energy can be defined as the difference in the free energy between the bulk material and the slab model per unit area. For a clean and symmetric slab surface, it is obtained as follows

$$\gamma^{\text{clean}} = \frac{1}{2S}\left[G^{\text{slab}} - G^{\text{bulk}}\right] \tag{1}$$

where S is the total surface area, G^{slab} is the Gibbs free energy of the surface, and G^{bulk} is the Gibbs free energy of the bulk. To investigate the effect of Li and O vacancies, the surface energy must be computed considering the species in excess or shortage and taking into account the effect of chemical potential for different species μ_i

$$\gamma^{\text{clean}} = \frac{1}{2S}\left[G^{\text{slab}} - G^{\text{bulk}} - \sum_i \Delta N_i \mu_i\right] \tag{2}$$

where ΔN_i is the variation of the number of atoms for species i from the surface to the bulk.

The Gibbs free energies were approximated by the DFT total energy of the clean surface and LCO bulk (neglecting the entropic contribution). In our study, the amount of Co remains constant, whereas the Li and O concentrations were altered. The reference for μ_{Li} was obtained from first principles using the bulk metal,[43] and the reference for μ_{O} was obtained from H_2O and H_2 as

$$\mu_{\text{O}} = \mu_{H_2O} - \mu_{H_2} - \Delta G_{\text{form}}^{H_2O} \tag{3}$$

According to previous studies,[55] this is indeed the relevant reference value for the possible formation of OH, which avoids the inaccuracy of the DFT value for O_2.[56,57] Note that, in eq 3, the references for μ_{H_2O} and μ_{H_2} were computed from DFT by taking into account the zero-point energy (ZPE) contribution, while $\Delta G_{\text{form}}^{H_2O}$ was taken as the experimental Gibbs formation energy of water in the gas phase at standard conditions.[55]

Finally, μ_{Li} was related to the voltage with respect to Li^+/Li

$$V = -\frac{\mu_A^{\text{cathode}} - \mu_A^{\text{anode}}}{zF} = -\frac{\mu_A - \mu_A^{\text{ref}}}{zF} \tag{4}$$

where z is the transferred charge, F is the Faraday constant, and A represents Li^+. Scanning the possible values for μ_{Li}, we could investigate the surface stability with respect to Li^+/Li voltage.

The formation energy of an O_{vac} was calculated accordingly as

$$E_{f,O_{\text{vac}}} = \left(E_{Li_xCoO_{2-y-z}} + zE_{\text{O}}\right) - \left(E_{Li_xCoO_{2-y}}\right) \tag{5}$$

where $E_{Li_xCoO_{2-y}}$ is the energy of the initial surface configuration before the O_{vac} formation, $E_{Li_xCoO_{2-y-z}}$ is the energy of the surface configuration after the O_{vac} generation, E_{O} is the μ_{O} according to eq 3, and x represents the Li^+ concentration. The y and z values are used to indicate the stoichiometry of O atoms at the surface configuration (before and after the O_{vac} formation), with $y + z$ ranging from 0 to 0.5. Note that positive values of $E_{f,O_{\text{vac}}}$ mean that the O_{vac} generation is not energetically favorable.

2.4. H^+ Adsorption and Surface Energies of H^+-Covered Slabs. When H^+ adsorbs at the surface, O sites are preferred due to the strong interaction between H and O atoms. As depicted in Figure 1, four different possibilities were considered in this work for the formation of OH bonds. Such a bond can be created at the most exposed surface layer (Top-O) and/or at the subsurface, i.e., at the most internal surface layers (Top-O down). By comparing the binding energy for both sites, the tendency of H^+ to be intercalated in the material can be observed. The last two possibilities involve the formation of two OH bonds at the same O-site. These configurations lead to the formation of a water molecule at the surface layer (H_2O) and/or at the subsurface (H_2O down), as a result of the interaction between two H^+ from the electrolyte and an O atom from the surface. Since the O sites may be nonequivalent depending on the surface structure and the Li^+ content, several adsorbed configurations were computed.

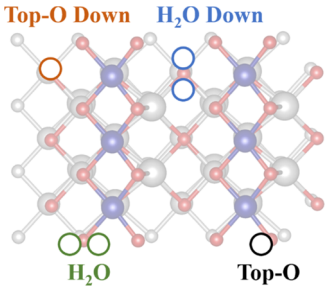

Figure 1. Schematic representation of the four possibilities considered for H^+ adsorption. Blue and red balls represent Co and O atoms, respectively. For the sake of clarity, the atoms of the unrelaxed layers have been depicted in gray.

The adsorption energy was calculated according to the following formula

$$E_{\text{ads}} = E_{\text{H/LCO}} - \left(E_{\text{LCO}} + \frac{n}{2}E_{H_2}\right) \tag{6}$$

where E_{LCO} is the energy of the pristine surface, n is the number of adsorbed H^+, E_{H_2} is the energy of the isolated H_2 molecule including the ZPE contribution, and $E_{\text{H/LCO}}$ is the energy of H^+ adsorbed on the corresponding LCO surface. $E_{\text{H/LCO}}$ also included the ZPE contribution, though considering only the vibrations of the adsorbates, i.e., protons. Note that the more negative the E_{ads}, the more favorable the interaction.

We investigated the surface energy after H^+ adsorption (γ^{cover}) at different H^+ coverages. γ^{cover} was calculated as the sum of the surface free energy of the clean surface (γ^{clean}) and the Gibbs free energy related to H^+ adsorption (γ^{ads})[58,59] as follows

$$\gamma^{\text{cover}} = \gamma^{\text{clean}} + \gamma^{\text{ads}} \tag{7}$$

Then, the adsorption surface free energy (γ^{ads}) was estimated as

$$\gamma^{\text{ads}} = \frac{1}{2S}\left[E^{\text{cover}} - E_{\text{LCO}}^{\text{slab}} - N_{\text{H}}\mu_{\text{H}}\right] \tag{8}$$

where E^{cover} is the energy of the LCO slab with the adsorbed H^+, and μ_{H} is calculated as in eq 6.

https://doi.org/10.1021/acs.jpcc.1c09348
J. Phys. Chem. C 2022, 126, 110−119

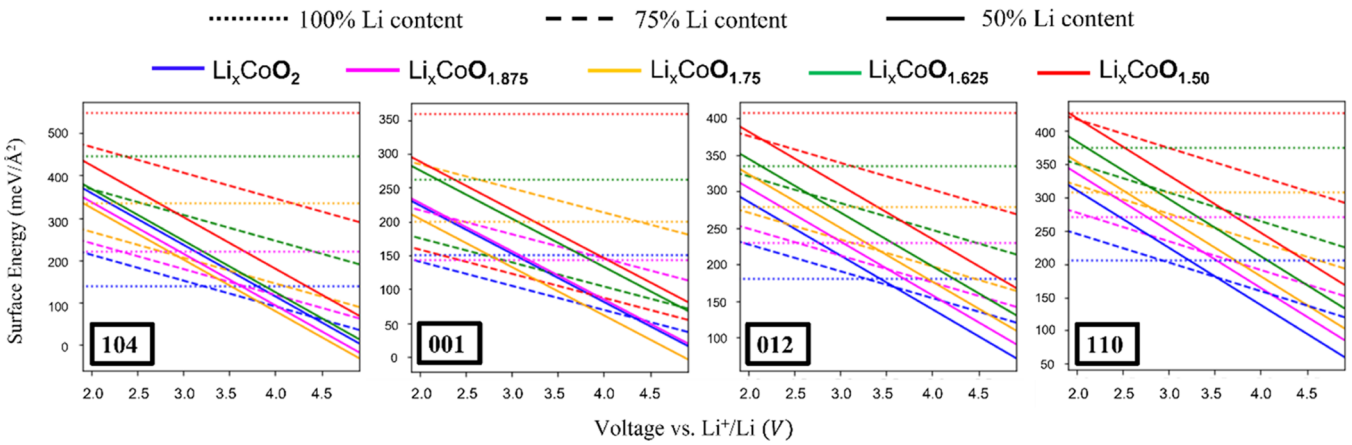

Figure 2. Surface energy (meV/Å^2) as a function of voltage versus Li$^+$/Li for the four different surface terminations of LCO with different Li$^+$ contents. Dotted, dashed, and solid lines represent full, 75%, and 50% Li coverage of the surface models, respectively, and different colors represent different concentrations of O_{vac} on the surface structure.

The role of H^+ in the O_{vac} formation was also investigated. In these cases, a OH moiety was removed after H^+ adsorption (OH_{vac}). The formation energy was calculated as

$$E_{OH_{vac}} = (E_{H_{k-z}Li_xCoO_{2-y-z}} - z\,E_{OH}) - (E_{H_kLi_xCoO_{2-y}}) \quad (9)$$

where $E_{H_k\,Li_x\,CoO_{2-y}}$ is the energy of the surface configuration with H^+ adsorbed ($0 \le k \le 0.5$), $E_{H_{k-z}\,Li_x\,CoO_{2-y-z}}$ is the energy of the surface after OH extraction, and E_{OH} is the energy of the OH moiety according to

$$E_{OH} = E_{H_2O} - \frac{1}{2}E_{H_2} \quad (10)$$

3. RESULTS

3.1. O_{vac} Formation and Stability of Clean Surfaces.

The stability of bare LCO surfaces has been investigated by comparing the stoichiometric slabs with surfaces that contain O_{vac}. Moreover, the surface energy has been analyzed as a function of Li$^+$/Li voltage. The latter controls the Li$^+$ content on the cathode material during the charge/discharge operations. We have explored several orderings of O_{vac} to find the lowest energy configurations (see Figures S2−S5 in the Supporting Information).

Figure 2 shows the surface energy at different O compositions as a function of Li$^+$/Li voltage for all of the fully and partially lithiated terminations considered in this work. As shown in Figure S6, the surface energy has been plotted as a function of Li$^+$ content per each studied slab termination. In general terms, the O_{vac}-free configurations (blue lines) are most stable for most studied surfaces. This can be directly related to the possible change in the Co local coordination environments after the O_{vac} formation, which strongly affects the surface energy. On the other hand, as expected, our simulations predict a significant effect of Li$^+$/Li voltage on surface stability. The higher the voltage, the more stable the delithiated surfaces.

For the (104) termination, the partially delithiated configurations are more stable at voltages typically applied during battery operations (3.5−4.2 V vs Li$^+$/Li). Fully lithiated surfaces are energetically favored only below 3 V versus Li$^+$/Li. With respect to the O loss, Co coordination plays a key role. The most external Co atoms are 5-fold-coordinated, while the internal Co atoms remain 6-fold-coordinated prior to the O_{vac} formation. The latter causes a coordination loss to Co atoms placed at the most exposed layer. Consequently, the surface energy increases when more O_{vac} is generated on surfaces with Li contents of 100 and 75%. However, the O_{vac} generation is energetically favored for configurations with 50% Li since $Li_{0.50}CoO_{1.875}$ and $Li_{0.50}CoO_{1.75}$ surfaces have lower γ^{clean} than the O_{vac}-free slab (see Figure 2). Despite the reduction of Co coordination at the most external layer (to 4-fold coordination), the surface is reconstructed to minimize the γ^{clean}. As depicted in Figure 3a, after atomic relaxation, the O and Co

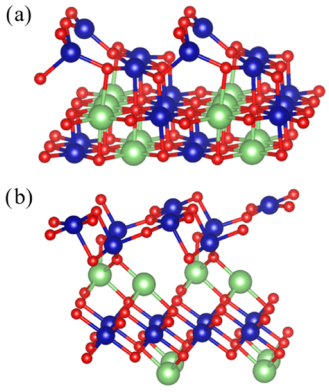

Figure 3. Ball-and-stick representation of the $Li_{0.50}CoO_{1.75}$ (a) (104) and (b) (001) surfaces. Li, Co, and O atoms are depicted in green, blue, and red, respectively.

atoms are not anymore in the same layer. The Co atoms, which were initially placed at the most exposed layer, slightly move downward, forming 4-fold-coordinated Co. The predicted O loss may be related to Li vacancies and the Co valence since the formation of O_{vac} leads to the reduction of transition metal cations.[34] The $Li_{0.50}CoO_2$ configuration has mixed Co^{4+}/Co^{3+} oxidation states. The O loss reduces Co^{4+} to Co^{3+} and may explain the lower γ^{clean} in comparison to the stoichiometric $Li_{0.50}CoO_2$ configuration. Our simulations predict the formation of O_{vac} on the half-lithiated configurations at voltages superior to 3.7 V versus Li$^+$/Li.

For the (001) surface, we found that partially lithiated surfaces are lower in energy than the fully lithiated ones at voltages superior to 2 V. With respect to fully lithiated surfaces,

https://doi.org/10.1021/acs.jpcc.1c09348
J. Phys. Chem. C 2022, 126, 110−119

the formation of one O_{vac}−$LiCoO_{1.875}$− competes with the O_{vac}-free configuration. At this surface, the Co atoms are 6-fold-coordinated, like in LCO bulk. The formation of one O_{vac} entails the combination of 6- and 5-fold-coordinated Co atoms at the most exposed surface layer. Configurations with less O content have the largest surface energies because the exposed Co atoms are 1- or 2-fold-coordinated (see Figure S3). On the other hand, the formation of O_{vac} is not favored in compositions with 75% Li content. The O_{vac}-free configuration has the lowest γ^{clean} and is the most stable surface at voltages below 3.7 V versus Li^+/Li. Regarding the half-lithiated structures, surface reconstruction is observed. Some of the Co atoms placed below the exposed O atoms moved upward during atomic relaxation in the $Li_{0.50}CoO_{1.75}$ configuration, generating two Co layers (see Figure 3b). The most exposed layer consists of alternating 4- and 5-fold-coordinated Co atoms, which minimize the γ^{clean}. This reconstructed surface is predicted to be the lowest energy surface above 3.7 V versus Li^+/Li, which indicates that it is energetically favored to form O_{vac} on this surface termination. It is interesting to highlight that if Co atoms do not evolve toward 4-fold coordination, forming tetrahedra, the surface energy increases. As it was predicted for the (104) termination, the formation of CoO_4 tetrahedra after the O_{vac} generation and surface reconstruction is energetically favorable with respect to 5-fold coordination.

On the other hand, one might expect the O_{vac} formation to be energetically favored at the terminations with high γ^{clean}. This is, however, not the case for the (012) and (110) surfaces. Originally, Co atoms are 4-fold-coordinated to O atoms at the most exposed layer for both surfaces.[41] The generation of O_{vac} and the subsequent reconstruction leads to the formation of structures with very low coordinated Co atoms at the most exposed surface. These reconstructions occur for fully and partially lithiated stoichiometries (see Figures S4 and S5 in the Supporting Information).

Our computations show that the Li vacancies, Co coordination, and charge ordering have an important impact on γ^{clean} and the stabilization of O_{vac}. The lowest energy terminations—(104) and (001)—and therefore the most exposed ones have more tendency to lose O and occur at half-lithiated surfaces. These terminations have lower γ^{clean} after the surface reconstruction favors the 4-fold Co coordination.

3.2. H^+ Adsorption on Li_xCoO_2 Surfaces. We also investigated the adsorption of H^+ on Li_xCoO_2 surfaces. A systematic study was carried out to analyze the binding energy and structural effects from low to high H^+ coverage. Here, the H^+ coverage regime (Θ_H) is indicated by the number of H^+ per number of O atoms on the most exposed surface layer. Table 1 reports the adsorption energy per H^+ adsorbed for all of the coverages and its respective adsorption site for the lowest energy configuration. Tables S1−S4 in the Supporting Information list a few more ground states for each termination, and Figures S7−S10 illustrate the sketches of the most favorable structures after H^+ adsorption.

For the (104) surface, the binding energy of H^+ increases (more negative) as the surface gets delithiated. As expected, the most favorable adsorption site is on top of the most external O surface atoms forming hydroxyl groups (OH). The OH formation can be characterized by the computed vibrational frequencies for the adsorbed H^+ atoms, typically ranging from 3200 to 3700 cm^{-1}. On the other hand, the H^+ adsorption on the most internal layers (Top-O down) competes with the adsorption on the most exposed layer for $Li_{0.5}CoO_2$ configurations. The adsorbed H^+ on the internal layers is placed at Li^+ vacancy sites, forming hydroxyl groups with vicinal O atoms. As a result, the Co atoms located on the second layer move upward between the first and second layers, becoming 4-fold coordinated (Figure 4a). It is proved that the presence of H^+ is preferable with respect to Li^+ due to the stable O−H bond formation, and it negatively affects the Li^+ (re)insertion/extraction, which is detrimental for the cathode

Table 1. H^+ Coverage (Θ_H (%)), Adsorption Energy per H^+ (E_{ads}/H^+ (eV)) and Adsorption Site of the Most Favorable Configurations after H^+ Adsorption

Ter	surface	Θ_H (%)	E_{ads}/H^+ (eV)	site
(104)	$LiCoO_2$	25	−0.97	Top-O
		50	−0.94	Top-O
		75	−1.20	Top-O
		100	−0.45	Top-O
	$Li_{0.75}CoO_2$	25	−1.47	Top-O
		50	−1.38	Top-O
		75	−1.35	Top-O
		100	−1.28	Top-O
	$Li_{0.5}CoO_2$	25	−2.77	Top-O
		50	−2.01	Top-O
		75	−2.03	Top-O
		100	−1.67	Top-O up/down
(001)	$LiCoO_2$	25	−3.21	Top-O
		50	−1.55	Top-O
		75	−1.14	Top-O
		100	−1.18	Top-O
	$Li_{0.75}CoO_2$	25	−1.30	Top-O
		50	−1.40	Top-O
		75	−1.09	Top-O
		100	−0.88	H_2O
	$Li_{0.5}CoO_2$	25	−3.08	Top-O
		50	−2.81	Top-O
		75	−1.90	Top-O
		100	−1.21	Top-O
(110)	$LiCoO_2$	25	−1.61	Top-O
		50	−1.41	Top-O
		75	−1.23	Top-O
		100	−1.06	Top-O
	$Li_{0.75}CoO_2$	25	−1.99	Top-O
		50	−1.69	Top-O
		75	−1.45	Top-O
		100	−1.39	Top-O
	$Li_{0.5}CoO_2$	25	−1.61	Top-O
		50	−1.64	Top-O
		75	−1.69	Top-O
		100	−1.59	Top-O
(012)	$LiCoO_2$	25	−0.96	Top-O
		50	−1.26	Top-O
		75	−1.05	Top-O
		100	−0.82	Top-O
	$Li_{0.75}CoO_2$	25	−1.86	Top-O down
		50	−1.72	Top-O
		75	−1.61	Top-O
		100	−1.43	Top-O
	$Li_{0.5}CoO_2$	25	−1.93	Top-O down
		50	−1.75	Top-O up/down
		75	−1.70	Top-O up/down
		100	−1.67	Top-O up/down

https://doi.org/10.1021/acs.jpcc.1c09348
J. Phys. Chem. C 2022, 126, 110−119

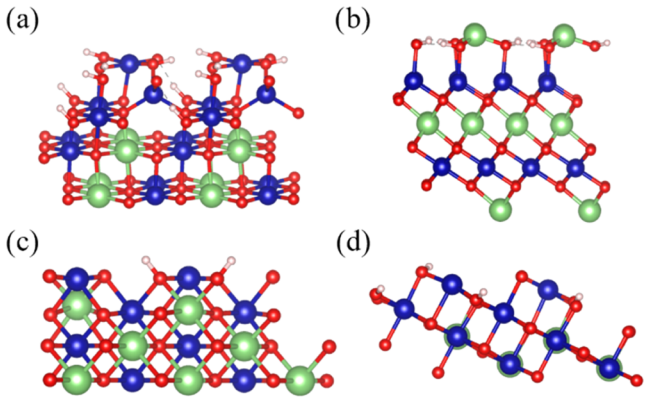

Figure 4. Ball-and-stick representation of (a) the $Li_{0.50}CoO_2$ (104) surface at 100% H^+ coverage, (b) the $LiCoO_2$ (001) surface at 100% H^+ coverage, (c) the $Li_{0.75}CoO_2$ (110) surface at 25% H^+ coverage, and (d) the $Li_{0.50}CoO_2$ (012) surface at 100% H^+ coverage. The color scheme is the same as in Figure 3.

performance.[18,28] Thus, (104) termination facilitated the H^+ intercalation on the material at voltages superior to 3.7 V versus Li^+/Li, where the half-delithiated surface predominates.

The largest binding energies are found for the (001) termination, where the adsorption of H^+preferably forms simple OH bonds on Top-O sites. Binding energies reported in Table 1 indicate that water formation can compete with a simple OH moiety only for a fully lithiated surface and at high H^+ coverage regime. In general, the binding energy of H^+ is more favorable at low coverages. Our simulations also reveal lower H^+ binding energies (less negative E_{ads}) on $Li_{0.75}CoO_2$ compared to fully and half-lithiated surfaces. This is related to the lower γ^{clean} of $Li_{0.75}CoO_2$ and the surface reconstruction observed on fully lithiated surfaces after H^+ adsorption (Figure 4b). The Li^+ ions move downward and H^+ forms hydroxyl groups parallel to the external surface layer. Moreover, the Co atoms become tetrahedral. It may be explained by the Co valence since the surface protonation at fully lithiated configurations implies the formation of Co^{2+}.

The H^+ interaction with the (110) termination follows the same tendency as for the (001) one, where the binding energy of H^+ is more favorable at a low coverage regime. Figure 4c illustrates the general behavior of this surface termination after H^+ adsorption, where H^+ form hydroxyl groups on Top-O sites perpendicular to the surface layers. As reported in Table 1, the adsorption energy of H^+ in the Top-O sites is preferred. In contrast, the adsorption on the most internal layers (Top-O down) is favorable for the half-lithiated (012) surface (Figure 4d). In Table 1, we observe that the lower the amount of Li^+ at the (012) surface, the higher the tendency to be adsorbed on the deepest layers. For the $Li_{0.75}CoO_2$ (012) termination, the H^+ adsorption on the subsurface layer is predicted to be most favorable. Again, as it is suggested for (104) slab, the H^+ intercalation on $LiCoO_2$ is predicted on (012) surfaces.

Our computations show that the H^+-LCO chemisorption is strong, especially at low coverage regime due to the formation of OH bonds. In general, the adsorption takes place on Top-O sites, perpendicularly to the surface. However, for some configurations, the H^+ are adsorbed parallel to the surface, forming OH bonds oriented toward the Li^+ vacancy sites. For the (104) and (012) terminations, the H^+ can be intercalated in the material, also forming OH bonds, and placed close to the most internal Li^+ vacancy sites. The H^+ insertion and the occupation of Li^+ vacancy sites are, a priori, undesirable due to the competition with Li^+, which may affect the Li^+ (re)-insertion and its diffusion on the material.[18]

3.3. Covered Surface Energies (γ^{cover}).

Figure 5 illustrates the surface energy after H^+ adsorption, γ^{cover}, at different O compositions as a function of Li^+/Li voltage. The number of adsorbed H^+ depends on the number of O atoms in the most exposed surface layer. Thus, O_{vac}-free surface models (Li_xCoO_2) can adsorb more H^+ than the surfaces with O_{vac} (Li_xCoO_{2-y}). In general, Figure 5 shows that the presence of H^+ allows the formation of Li^+ vacancies at lower voltages (3.0−3.2 V vs Li^+/Li) in comparison to bare surfaces, where the half-delithiation is predicted around 3.5−3.7 V versus Li^+/Li.

The surfaces with the lowest γ^{cover} correspond to configurations without O_{vac} independent of the surface termination. The adsorption of H^+ stabilizes the surface energy due to the highly favorable formation of OH bonds, and

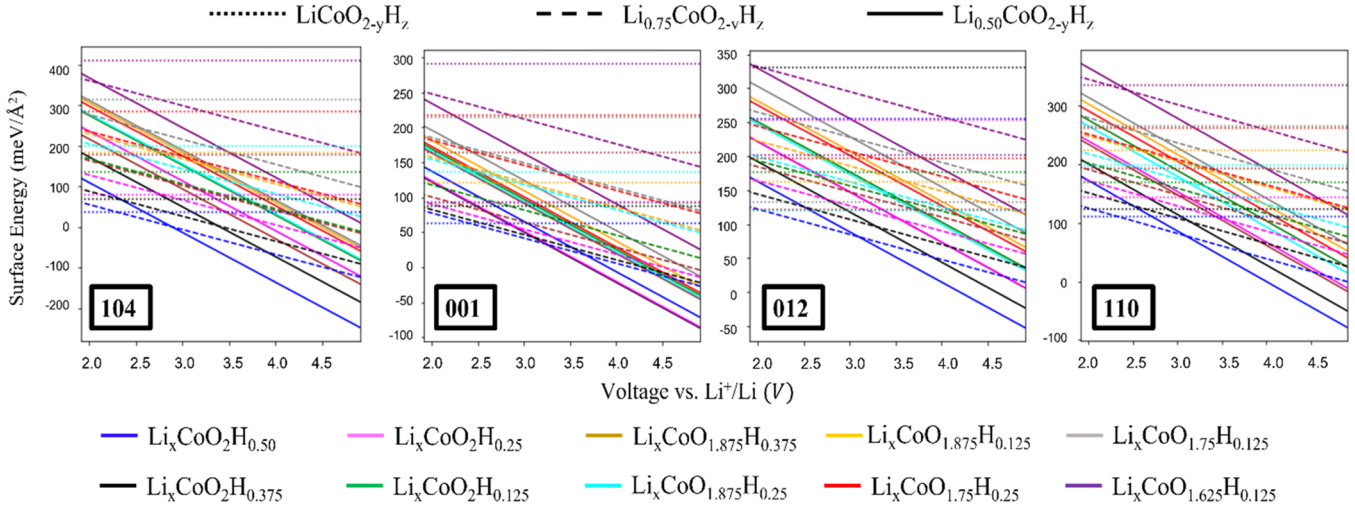

Figure 5. Surface energy (meV/Å^2) as a function of the voltage versus Li^+/Li of the four different surface terminations of LCO with different Li^+ contents after the H^+ adsorption. Dotted, dashed, and solid lines represent full, 75 and 50% Li concentration on surface models, respectively. Colored lines represent configurations with different concentrations of oxygen vacancies and different proton coverage.

https://doi.org/10.1021/acs.jpcc.1c09348
J. Phys. Chem. C 2022, 126, 110−119

consequently, configurations that maximize the number of OH moieties have the lowest γ^{cover}. As depicted in Figure 5, fully protonated surfaces without O_{vac} (blue lines) are the most stable configurations, except for the (001) termination, where the surface is partially protonated. In this particular case, $Li_{0.50}CoO_2H_{0.375}$ (solid black line) and $Li_{0.50}CoO_2H_{0.25}$ (solid magenta line) are the surfaces with the lowest γ^{cover}. Both configurations are degenerate in energy and are superposed in the plot. This result can be related to the surface geometry after H^+ adsorption. H^+ is bonded on Top-O sites perpendicularly to the surface maximizing the H^+-H^+ distance, except at full coverage, where an inclination of around 45° is observed, increasing the H^+-H^+ interaction (Figure S8).

With respect to O_{vac} formation, our simulations clearly show that H^+ plays the most relevant role in terms of surface energetics. The more the O atoms on the surface, the more stable the OH bonds, and, as consequence, the surface stabilization is larger on surfaces without O_{vac}.

3.4. Effect of H^+ on O Vacancy Formation. Considering the large surface stabilization that implies the interaction with H^+, it is important to investigate if O_{vac} can be generated after the H^+ adsorption or only on clean surface terminations. We have reported the energy needed to generate O_{vac} after the adsorption of H^+. O_{vac} has been generated removing O surface atoms with the bonded H^+ (OH_{vac}) considering the most favorable configurations at different Θ_H. The energy cost of OH_{vac} generation for different surfaces has been calculated following eq 10, and the results are listed in Table S5.

For the highest energy surface terminations—(110) and (012)—our results show that the adsorption of H^+ does not favor the formation of OH_{vac}. Again, the Co coordination becomes the most relevant factor to (de)stabilize the surface termination, as it was predicted on clean (110) and (012) slabs. The (110) termination may work as a H^+ reservoir, without implications in terms of O loss and surface reconstruction. Independent of Li^+ concentration and voltage, the presence of H^+ decreases the surface energy without being intercalated on the most internal layers. In other words, (110) is not strongly affected by H^+ since the only predicted effect is the stabilization of half-delithiated surfaces at lower voltages (~0.5 V less with respect to bare surfaces). Nevertheless, (012) might play a detrimental role in the cathode performance since H^+ can intercalate on the subsurface layer and it is energetically unfavored to remove it. The intercalated H^+ on (012) can hinder the Li^+ insertion/extraction process and promote the phase transition toward cobalt oxide spinels.[22,28,31]

The OH_{vac} formation is not energetically favored on the fully lithiated (104) configuration, as already observed on the clean surface. Notwithstanding, H^+ can facilitate the O_{vac} formation on partially lithiated (104) surfaces. As illustrated in Figure 6, generating two O_{vac} on the bare $Li_{0.75}CoO_2$ surface is not energetically favorable (1.55 eV/O_{vac}), whereas extracting two OH moieties from $Li_{0.75}CoO_2H_{0.25}$ has a negative reaction energy (−0.18 eV/OH_{vac}). Moreover, our simulations suggest that the presence of H^+ does not allow the formation of O_{vac} by just removing O atoms. The adsorption of H^+ can favor the extraction of OH moieties and simultaneously block the extraction of neighboring O atoms without adsorbed H^+. For instance, it is energetically favorable to create an O_{vac} on the $Li_{0.50}CoO_2$ configuration ($Li_{0.50}CoO_2 \rightarrow Li_{0.50}CoO_{1.75}$), whereas the same process with adsorbed H^+ ($Li_{0.50}CoO_2H_{0.25} \rightarrow Li_{0.50}CoO_{1.75}H_{0.25}$) has an energy cost of 1.15 eV/O_{vac} (see

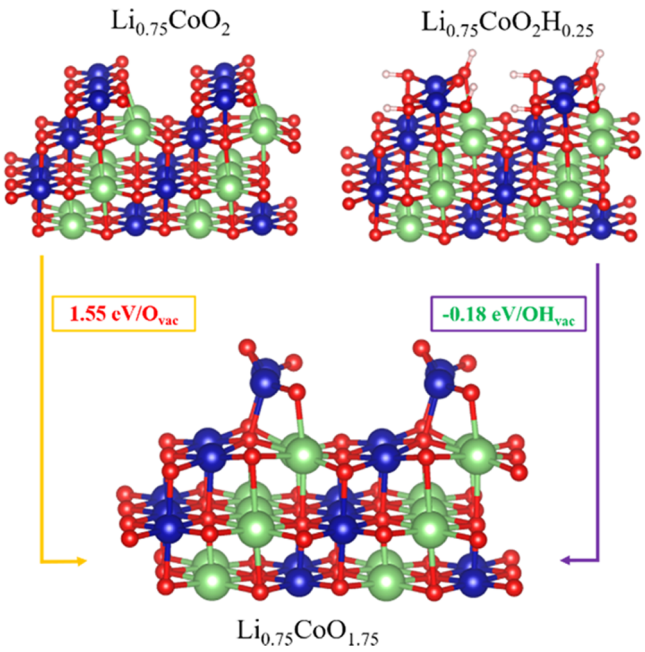

Figure 6. Ball-and-stick representation of $Li_{0.75}CoO_2$ (top left), $Li_{0.75}CoO_2H_{0.25}$ (top right), and $Li_{0.75}CoO_{1.75}$ (bottom) configurations of (104) termination. Orange and purple arrows represent the generation of O_{vac} and OH_{vac}, respectively. The color scheme is the same as in Figure 3.

Table S5). This fact is related to the intercalation of H^+ on the deepest surface layers. As previously described, the $Li_{0.50}CoO_2$ configuration of (104) termination can intercalate H^+ on the Top-O down sites. These adsorbed H^+ ions on the subsurface O atoms form large stable O−H−O hydrogen bonds, where the second O atom (without adsorbed H^+) is placed on the most external layer. To break these hydrogen bonds, high energy cost is required, hindering the formation of O_{vac} on the most external layers after the intercalation of H^+ in the material.

Finally, for the (001) termination, the same trend is observed as for the (104) surface. In general, removing OH moieties from fully and 75% lithiated surfaces comes with an energy cost. However, this tendency changes for 50% lithiated configurations. Figure 7 depicts the full reaction map that compares the energy needed to generate O_{vac} (orange) and OH_{vac} (purple) or to deprotonate the surface (cyan) on $Li_{0.50}CoO_{2-y}$ for the (001) termination. The results reported in Figure 7 show that the H^+ chemisorption facilitates the O loss. As an example, it is more favorable to generate two OH_{vac} ($Li_{0.50}CoO_2H_{0.50} \rightarrow Li_{0.50}CoO_{1.75}H_{0.25}$), with a formation energy of 2.50 eV (1.02 eV for the first OH extraction and 1.48 eV for the second one) than to create oxygen vacancies on clean slabs.

On the other hand, the formation of O_{vac} on $H^+-Li_{0.50}CoO_2$ stoichiometries (orange ways, bottom part) is unlikely due to the large formation energy (2.45, 1.73, 1.35, and 1.05 eV/O_{vac}). Note that the energy cost to generate an O_{vac} decreases when the H^+ coverage also decreases. This may be explained due to the formation of hydrogen bonds. At full H^+ coverages, it is observed that some adsorbed H^+ point to the vicinal O atoms on the surface. Consequently, it increases the cost to extract O atoms since the presence of adsorbed H^+ blocks the extraction of an adjacent O atom.

https://doi.org/10.1021/acs.jpcc.1c09348
J. Phys. Chem. C 2022, 126, 110−119

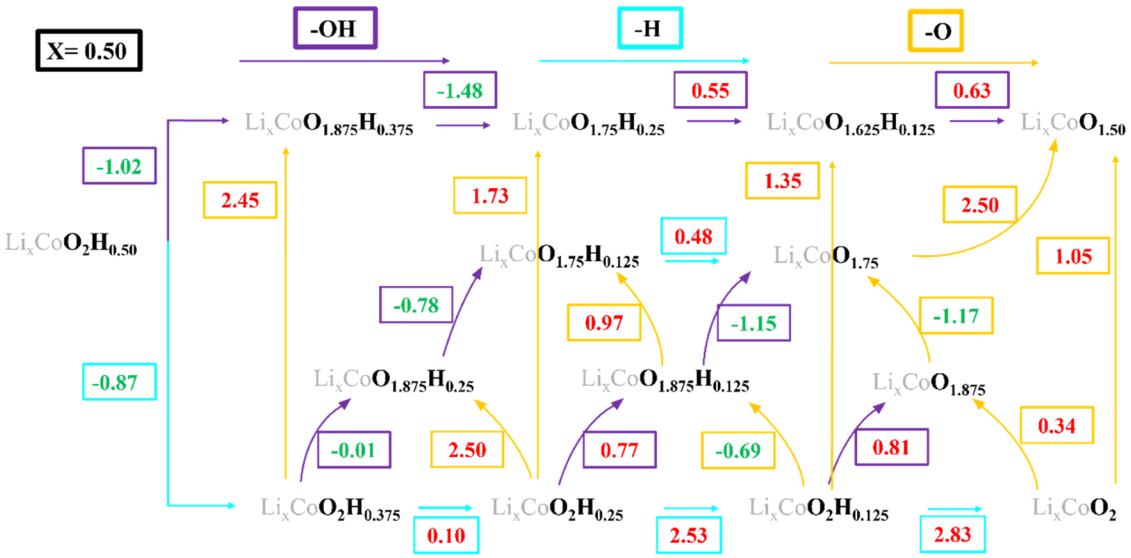

Figure 7. Reaction map for the protonated $Li_{0.50}CoO_2$ (001) surface. Orange, purple, and cyan arrows and boxes refer to the generation of O_{vac}, OH_{vac}, and deprotonation, respectively. Energies (eV) in red and green represent unfavorable and favorable processes, respectively. The energies for the orange path are in eV/O_{vac}.

One may conclude that the interaction of LCO with aqueous electrolytes facilitates the formation of O_{vac} due to the generation of OH moieties, albeit one must keep in mind that the lowest energy terminations—(001) and (104)—tend to be reconstructed and lose O without proton implication. On the other hand, it is proved that Li^+ vacancies favor O_{vac} and OH_{vac}, although on (104) and (012) terminations, H^+ remains adsorbed on the subsurface layers. This fact hinders the formation of O_{vac} due to the formation of hydrogen bonds and the difficulty to remove O from the deepest layers.

4. CONCLUSIONS

We carried out a DFT investigation of four different LCO surfaces focusing on the stability of O_{vac} and the effect of H^+ adsorption. For each surface, we considered three models with different Li^+ concentrations to mimic the effect of the charge/discharge process on battery operations. Co coordination is suggested as the key factor for surface stability since the O_{vac} formation depends on Co coordination and geometry after the surface reconstruction. Surface terminations that maximize the Co coordination are most energetically favorable. The formation of CoO_4 tetrahedra has been predicted on stable surfaces that contain O_{vac}. The generation of O_{vac} typically occurs on the most exposed surface terminations—(104) and (001)—due to surface reconstruction and beyond 3.7 V versus Li^+/Li.

We found that the binding energy of H^+ can be strong/moderate depending on the coverage. Most often, the adsorption of H^+ takes place on Top-O sites, forming OH moieties on the uppermost layer of the surface. For most configurations, the resulting OH groups are perpendicular to the surface. They can, however, be parallel to the surface when H^+ partially occupies Li^+ vacancy sites. On the other hand, for (104) and (012), H^+ can be intercalated in the subsurface layers at half-lithiated stoichiometries. For these configurations, H^+ bonds to the most internal O atoms close to Li^+ vacancy sites, which can drastically affect Li^+ insertion/extraction. Thus, our work suggests avoiding the use of these surface terminations to limit the possible H^+ intercalation.

In addition, our computations have shown that the presence of H^+ does not help the O_{vac} formation on terminations with large surface energy—(110) and (012) for LCO—since generating O_{vac} on (012) and (110) terminations is not energetically favorable for either the clean or H^+-covered surfaces. In contrast, on the lowest energy surfaces—(001) and (104) for LCO—H^+ can facilitate the formation of O_{vac} on O atoms bonded to protons. Nevertheless, the DFT results also show the double role of H^+, discouraging the formation of single O_{vac}. In other words, after the H^+ adsorption, OH moieties can be removed but H^+ can block the extraction of single O atoms close to OH moieties.

In any case, one must consider that the O_{vac} generation is energetically favored on bare surfaces as well. Thus, our simulations suggest that the O_{vac} formation is not dependent on the presence of H^+, i.e., the use of aqueous electrolytes. We observed a major dependence on the Co coordination and the Li^+ content since Li^+ vacancies favor the O_{vac} formation.

In summary, we predicted that O_{vac} is energetically favorable on the most exposed surfaces independent of H^+ adsorption, especially when these terminations contain Li^+ vacancies. In addition, we suggest the intercalation of H^+ on the subsurface layers on some partially lithiated configurations (104 and 012 terminations), which is not desirable. By exploring the behavior of several surface terminations of the LCO cathode material, our work has detailed that the O_{vac} formation and the effect of H^+ on the surface structure can be managed to control the crystal growth and the applied voltage. This is important to improve cathode stability and battery performance.

■ ASSOCIATED CONTENT

Supporting Information

The Supporting Information is available free of charge at https://pubs.acs.org/doi/10.1021/acs.jpcc.1c09348.

Ball-and-stick representation of four different LCO surfaces (fully and partially lithiated) considered in this work with different concentrations of oxygen vacancies; surface energies of fully and partially lithiated surfaces as a function of Li/Li^+ voltage, comparing the effect of the

https://doi.org/10.1021/acs.jpcc.1c09348
J. Phys. Chem. C 2022, 126, 110−119

oxygen vacancy formation; ball-and-stick representation of proton adsorption on LCO surfaces at different coverages; reported binding energies and adsorption sites of proton adsorption at different coverages on fully and partially lithiated LCO surfaces; and formation energy of OH vacancies on LCO surfaces (PDF)

AUTHOR INFORMATION

Corresponding Author

Gian-Marco Rignanese − *Institute of Condensed Matter and Nanosciences, UCLouvain, B-1348 Louvain-la-Neuve, Belgium;* orcid.org/0000-0002-1422-1205; Email: gian-marco.rignanese@uclouvain.be

Authors

Sergio Posada-Pérez − *Institute of Condensed Matter and Nanosciences, UCLouvain, B-1348 Louvain-la-Neuve, Belgium;* orcid.org/0000-0003-4200-4264

Geoffroy Hautier − *Institute of Condensed Matter and Nanosciences, UCLouvain, B-1348 Louvain-la-Neuve, Belgium; Thayer School of Engineering, Dartmouth College, Hanover, New Hampshire 03755, United States*

Complete contact information is available at: https://pubs.acs.org/10.1021/acs.jpcc.1c09348

Notes

The authors declare no competing financial interest.

ACKNOWLEDGMENTS

S.P.P., G.-M.R., and G.H. are grateful to the F.R.S.-FNRS for financial support. G.H. acknowledges the Communauté Francaise de Belgique for the support under Grant ARC 18/23-093. Computational resources were provided by the supercomputing facilities of the UCLouvain (CISM) and the Consortium des Equipements de Calcul Intensif en Fédération Wallonie-Bruxelles (CECI) funded by the Fonds de la Recherche Scientifique de Belgique (F.R.S.-FNRS) under Convention No. 2.5020.11.

REFERENCES

(1) Xie, J.; Lu, Y. C. A Retrospective on Lithium-Ion Batteries. *Nat. Commun.* **2020**, *11*, No. 2499.

(2) Wu, F.; Maier, J.; Yu, Y. Guidelines and Trends for Next-Generation Rechargeable Lithium and Lithium-Ion Batteries. *Chem. Soc. Rev.* **2020**, *49*, 1569−1614.

(3) Chao, D.; Zhou, W.; Xie, F.; Ye, C.; Li, H.; Jaroniec, M.; Qiao, S. Roadmap for Advanced Aqueous Batteries: From Design of Materials to Applications. *Sci. Adv.* **2020**, *6*, No. eaba4098.

(4) Arbizzani, C.; Gabrielli, G.; Mastragostino, M. Thermal Stability and Flammability of Electrolytes for Lithium-Ion Batteries. *J. Power Sources* **2011**, *196*, 4801−4805.

(5) Roth, E. P.; Orendorff, C. J. How Electrolytes Influence Battery Safety. *Electrochem. Soc. Interface* **2012**, *21*, 45−49.

(6) Kim, H.; Hong, J.; Park, K. Y.; Kim, H.; Kim, S. W.; Kang, K. Aqueous Rechargeable Li and Na Ion Batteries. *Chem. Rev.* **2014**, *114*, 11788−11827.

(7) Li, W.; Dahn, J. R.; Wainwright, D. S. Rechargeable Lithium Batteries with Aqueous Electrolytes. *Science* **1994**, *264*, 1115−1118.

(8) Smith, L.; Dunn, B. Opening the Window for Aqueous Electrolytes. *Science* **2015**, *350*, 918.

(9) Chang, Z.; Li, C.; Wang, Y.; Chen, B.; Fu, L.; Zhu, Y.; Zhang, L.; Wu, Y.; Huang, W. A Lithium Ion Battery Using an Aqueous Electrolyte Solution. *Sci. Rep.* **2016**, *6*, No. 28421.

(10) Tomiyasu, H.; Shikata, H.; Takao, K.; Asanuma, N.; Taruta, S.; Park, Y. Y. An Aqueous Electrolyte of the Widest Potential Window and Its Superior Capability for Capacitors. *Sci. Rep.* **2017**, *7*, No. 45048.

(11) Wan, F.; Zhu, J.; Huang, S.; Niu, Z. High-Voltage Electrolytes for Aqueous Energy Storage Devices. *Batteries Supercaps* **2020**, *3*, 323−330.

(12) Xie, J.; Liang, Z.; Lu, Y. C. Molecular Crowding Electrolytes for High-Voltage Aqueous Batteries. *Nat. Mater.* **2020**, *19*, 1006−1011.

(13) Suo, L.; Borodin, O.; Gao, T.; Olguin, M.; Ho, J.; Fan, X.; Luo, C.; Wang, C.; Xu, K. "Water-in-Salt" Electrolyte Enables High-Voltage Aqueous Lithium-Ion Chemistries. *Science* **2015**, *350*, 938−943.

(14) Suo, L.; Borodin, O.; Wang, Y.; Rong, X.; Sun, W.; Fan, X.; Xu, S.; Schroeder, M. A.; Cresce, A. V.; Wang, F.; et al. "Water-in-Salt" Electrolyte Makes Aqueous Sodium-Ion Battery Safe, Green, and Long-Lasting. Advanced Energy. *Materials* **2017**, *7*, No. 1701189.

(15) Vatamanu, J.; Borodin, O. Ramifications of Water-in-Salt Interfacial Structure at Charged Electrodes for Electrolyte Electrochemical Stability. *J. Phys. Chem. Lett.* **2017**, *8*, 4362−4367.

(16) Wang, Y.; Meng, X.; Sun, J.; Liu, Y.; Hou, L. Recent Progress in "Water-in-Salt" Electrolytes Toward Non-Lithium Based Rechargeable Batteries. *Front. Chem.* **2020**, *8*, No. 595.

(17) Shu, Q.; Chen, L.; Xia, Y.; Gong, X.; Gu, X. Proton-Induced Dysfunction Mechanism of Cathodes in an Aqueous Lithium Ion Battery. *J. Phys. Chem. C* **2013**, *117*, 6929−6932.

(18) Gu, X.; Liu, J. L.; Yang, J. H.; Xiang, H. J.; Gong, X. G.; Xia, Y. Y. First-Principles Study of H+ Intercalation in Layer-Structured $LiCoO_2$. *J. Phys. Chem. C* **2011**, *115*, 12672−12676.

(19) Wang, Y.; Luo, J.; Wang, C.; Xia, Y. Hybrid Aqueous Energy Storage Cells Using Activated Carbon and Lithium-Ion Intercalated Compounds. *J. Electrochem. Soc.* **2006**, *153*, A1425.

(20) Mizushima, K.; Jones, P. C.; Wiseman, P. J.; Goodenough, J. B. A new Cathode Material for Batteries of High Energy Density. *Mater. Res. Bull.* **1980**, *15*, 783−789.

(21) Tang, W.; Zhu, Y.; Hou, Y.; Liu, L.; Wu, Y.; Loh, K. P.; Zhang, H.; Zhu, K. Aqueous Rechargeable Lithium Batteries as an Energy Storage System of Superfast Charging. *Energy Environ. Sci.* **2013**, *6*, 2093−2104.

(22) Fernández-Rodríguez, J.; Hernan, L.; Morales, J.; Tirado, J. Low-Temperature Hydrothermal Transformations of $LiCoO_2$ and $HCoO_2$. *Mater. Res. Bull.* **1988**, *23*, 899−904.

(23) Gupta, R.; Manthiram, A. Chemical Extraction of Lithium from Layered $LiCoO_2$. *J. Solid State Chem.* **1996**, *121*, 483−491.

(24) Choi, J.; Alvarez, E.; Arunkumar, T. A.; Manthiram, A. Proton Insertion into Oxide Cathodes during Chemical Delithiation. *Electrochem. Solid-State Lett.* **2006**, *9*, No. A241.

(25) Benedek, R.; Thackeray, M. M.; van de Walle, A. Free Energy for Protonation Reaction in Lithium-Ion Battery Cathode Materials. *Chem. Mater.* **2008**, *20*, 5485−5490.

(26) Medina, E. A.; Aleksandrova, I.; Karppinen, M. Proton Intercalation into Different CoO_2 Layer Matrices. *J. Solid State Chem.* **2019**, *278*, No. 120899.

(27) Guduru, R. K.; Icaza, J. C. A Brief Review on Multivalent Intercalation Batteries with Aqueous Electrolytes. *Nanomaterials* **2016**, *6*, No. 41.

(28) Posada-Pérez, S.; Rignanese, G. M.; Hautier, G. Influence of Stacking on H^+ Intercalation in Layered $ACoO_2$(A = Li, Na) Cathode Materials and Implications for Aqueous Li-Ion Batteries: A First-Principles Investigation. *Chem. Mater.* **2021**, *33*, 6942−6954.

(29) Oh, H.; Yamagishi, H.; Ohta, T.; Byon, H. R. Understanding the Interfacial Reactions of $LiCoO_2$ positive Electrodes in Aqueous Lithium-Ion Batteries. *Mater. Chem. Front.* **2021**, *5*, 3657−3663.

(30) Ruffo, R.; Wessells, C.; Huggins, R. A.; Cui, Y. Electrochemical Behavior of $LiCoO_2$ as Aqueous Lithium-Ion Battery Electrodes. *Electrochem. Commun.* **2009**, *11*, 247−249.

(31) Ramanujapuram, A.; Gordon, D.; Magasinski, A.; Ward, B.; Nitta, N.; Huang, C.; Yushin, G. Degradation and Stabilization of Lithium Cobalt Oxide in Aqueous Electrolytes. *Energy Environ. Sci.* **2016**, *9*, 1841−1848.

(32) Wang, Y.; Xiao, X.; Li, Q.; Pang, H. Synthesis and Progress of New Oxygen-Vacant Electrode Materials for High-Energy Rechargeable Battery Applications. *Small* **2018**, *14*, No. 1802193.
(33) Gao, R.; Liu, L.; Hu, Z.; Zhang, P.; Cao, X.; Wang, B.; Liu, X. The Role of Oxygen Vacancies in Improving the Performance of CoO as Bifunctional Cathode catalyst for Rechaergable Li-O2 Batteries. *J. Mater. Chem. A* **2015**, *3*, 17598−17605.
(34) Tang, Z. K.; Xue, Y. F.; Teobaldi, G.; Liu, L. M. The Oxygen Vacancy in Li-Ion Battery Cathode Materials. *Nanoscale Horiz.* **2020**, *5*, 1453−1466.
(35) Hausbrand, R.; Cherkashinin, G.; Ehrenberg, H.; Gröting, M.; Albe, K.; Hess, C.; Jaegermann, W. Fundamental Degradation Mechanisms of Layered Oxide Li-Ion Battery Cathode Materials: Methodology, Insights and Novel Approaches. *Mater. Sci. Eng., B* **2015**, *192*, 3−25.
(36) Lee, S.; Jin, W.; Kim, S. H.; Joo, S. H.; Nam, G.; Oh, P.; Kim, Y. K.; Kwak, S. K.; Cho, J. Oxygen Vacancy Diffusion and Condensation in Lithium-Ion Battery Cathode Materials. *Angew. Chem., Int. Ed.* **2019**, *58*, 10478−10485.
(37) Hinuma, Y.; Toyao, T.; Kamachi, T.; Maeno, Z.; Takakusagi, S.; Furukawa, S.; Takigawa, I.; Shimizu, K. I. Density Functional Theory Calculations of Oxygen Vacancy Formation and Subsequent Molecular Adsorption on Oxide Surfaces. *J. Phys. Chem. C* **2018**, *122*, 29435−29444.
(38) Hu, W.; Wang, H.; Luo, W.; Xu, B.; Ouyang, C. Formation and Thermodynamic Stability of Oxygen Vacancies in Typical Cathode Materials for Li-Ion Batteries: Density Functional Theory Study. *Solid State Ionics* **2020**, *347*, No. 115257.
(39) Cherkashinin, G.; Jaegermann, W. Dissociative Adsorption of H_2O on $LiCoO_2$ (00l) Surfaces: Co Reduction Induced by Electron Transfer from Intrinsic Defects. *J. Chem. Phys.* **2016**, *144*, No. 184706.
(40) Maram, P. S.; Costa, G. C. C.; Navrotsky, A. Experimental Confirmation of Low Surface Energy in $LiCoO_2$ and Implications for Lithium Battery Electrodes. *Angew. Chem., Int. Ed.* **2013**, *52*, 12139−12142.
(41) Perdew, J. P.; Burke, K.; Ernzerhof, M. Generalized Gradient Approximation Made Simple. *Phys. Rev. Lett.* **1996**, *77*, 3865−3868.
(42) Dudarev, S.; Botton, G. Electron-Energy-Loss Spectra and the Structural Stability of Nickel Oxide: An LSDA+U Study. *Phys. Rev. B: Condens. Matter Mater. Phys.* **1998**, *57*, No. 1505.
(43) Jain, A.; Ong, S. P.; Hautier, G.; Chen, W.; Richards, W. D.; Dacek, S.; Cholia, S.; Gunter, D.; Skinner, D.; Ceder, G.; et al. Commentary: The Materials Project: A Materials Genome Approach to Accelerating Materials Innovation. *APL Mater.* **2013**, No. 011002.
(44) Blöchl, P. E. Projector Augmented-Wave Method. *Phys. Rev. B: Condens. Matter Mater. Phys.* **1994**, *50*, 17953−17979.
(45) Kresse, G.; Joubert, D. From Ultrasoft Pseudopotentials to the Projector Augmented-Wave Method. *Phys. Rev. B: Condens. Matter Mater. Phys.* **1999**, *59*, 1758−1775.
(46) Pack, J. D.; Monkhorst, H. J. "special Points for Brillouin-Zone Integrations"-a Reply. *Phys. Rev. B: Condens. Matter Mater. Phys.* **1977**, *16*, 1748−1749.
(47) Kresse, G.; Furthmüller, J. Efficient Iterative Schemes for Ab Initio Total-Energy Calculations Using a Plane-Wave Basis Set. *Phys. Rev. B: Condens. Matter Mater. Phys.* **1996**, *54*, 11169−11186.
(48) Kramer, D.; Ceder, G. Tailoring the Morphology of $LiCoO_2$: A First Principles Study. *Chem. Mater.* **2009**, *21*, 3799−3809.
(49) Moradabadi, A.; Kaghazchi, P. Mechanism of Li Intercalation/Deintercalation into/from the Surface of $LiCoO_2$. *Phys. Chem. Chem. Phys.* **2015**, *17*, 22917−22922.
(50) Hong, L.; Hu, L.; Freeland, J. W.; Cabana, J.; Ögüt, S.; Klie, R. F. Electronic Structure of $LiCoO_2$ Surfaces and Effect of Al Substitution. *J. Phys. Chem. C* **2019**, *123*, 8851−8858.
(51) Wang, L.; Zhou, F.; Meng, Y. S.; Ceder, G. First-Principles Study of Surface Properties of $LiFePO_4$: Surface Energy, Structure, Wulff Shape, and Surface Redox Potential. *Phys. Rev. B: Condens. Matter Mater. Phys.* **2007**, *76*, No. 165435.
(52) Tasker, P. W. The Stability of Ionic Crystal Surfaces. *J. Phys. C: Solid State Phys.* **1979**, *12*, 4977−4984.
(53) Hu, L.; Xiong, Z.; Ouyang, C.; Shi, S.; Ji, Y.; Lei, M.; Wang, Z.; Li, H.; Huang, X.; Chen, L. Ab Initio Studies on the Stability and Electronic Structure of $LiCoO_2$ (003) Surfaces. *Phys. Rev. B: Condens. Matter Mater. Phys.* **2005**, *71*, No. 125433.
(54) Van der Ven, A.; Aydinol, M. K.; Ceder, G. First-Principles Evidence for Stage Ordering in Li_xCoO_2. *J. Electrochem. Soc.* **1998**, *145*, 2149−2155.
(55) Kolb, M. J.; Calle-Vallejo, F.; Juurlink, L. B. F.; Koper, M. T. M. Density Functional Theory Study of Adsorption of H_2O, H, O, and OH on Stepped Platinum Surfaces. *J. Chem. Phys.* **2014**, *140*, No. 134708.
(56) Calle-Vallejo, F.; Martínez, J. I.; García-Lastra, J. M.; Mogensen, M.; Rossmeisl, J. Trends in Stability of Perovskite Oxides. *Angew. Chem., Int. Ed.* **2010**, *49*, 7699−7701.
(57) Martínez, J. I.; Hansen, H. A.; Rossmeisl, J.; Nørskov, J. K. Formation Energies of Rutile Metal Dioxides Using Density Functional Theory. *Phys. Rev. B: Condens. Matter Mater. Phys.* **2009**, *79*, No. 045120.
(58) Reuter, K.; Scheffler, M. First-Principles Atomistic Thermodynamics for Oxidation Catalysis: Surface Phase Diagrams and Catalytically Interesting Regions. *Phys. Rev. Lett.* **2003**, *90*, No. 046103.
(59) Reuter, K.; Scheffler, M. Composition, Structure, and Stability of RuO_2 (110) as a Function of Oxygen Pressure. *Phys. Rev. B: Condens. Matter Mater. Phys.* **2002**, *65*, No. 035406.

https://doi.org/10.1021/acs.jpcc.1c09348
J. Phys. Chem. C 2022, 126, 110−119